Research article

S. Hamed Shams Mousavi, Robert Lemasters, Feng Wang, Ali Eshaghian Dorche, Hossein Taheri, Ali A. Eftekhar, Hayk Harutyunyan* and Ali Adibi*

Phase-matched nonlinear second-harmonic generation in plasmonic metasurfaces

https://doi.org/10.1515/nanoph-2018-0181
Received October 24, 2018; revised January 17, 2019; accepted January 21, 2019

Abstract: The phase matching between the propagating fundamental and nonlinearly generated waves plays an important role in the efficiency of the nonlinear frequency conversion in macroscopic crystals. However, in nanoscale samples, such as nanoplasmonic structures, the phase-matching condition is often ignored due to the sub-wavelength nature of the materials. Here, we first show that the phase matching of the lattice plasmon modes at the fundamental and second-harmonic frequencies in a plasmonic nanoantenna array can effectively enhance the surface-enhanced second-harmonic generation. Additionally, a significant enhancement of the second-harmonic generation is demonstrated using stationary band-edge lattice plasmon modes with zero phase.

Keywords: plasmonics; metasurface; nanoantenna; nonlinear optics; second harmonic generation.

1 Introduction

Nonlinear optical effects are the key underlying processes in a host of advanced photonic functionalities such as all-optical signal processing [1, 2], photon entanglement [3], generation of optical qubits for quantum computing [4] and quantum cryptography [5, 6], generation of ultrashort pulses [7, 8], generation of optical solitons and optical combs [9, 10], as well as nonlinear spectroscopy [11, 12] and imaging [13–15] techniques. The high field enhancement in plasmonic nanostructures and metasurfaces (MSs) enables us to achieve relatively efficient nonlinear signal generation in sub-wavelength volumes. Nevertheless, improving the nonlinear frequency conversion efficiency in these structures remains a critical primary challenge [16] in many applications including nanomedicine [17, 18], nonlinear biosensing [19–21], surface-enhanced nonlinear spectroscopy and imaging [22–26] and generation of ultrashort pulses at the extreme ultraviolet spectral range [27–29].

Achieving efficient nonlinear signal conversion in nonlinear nano-optic devices requires high field enhancement in both excitation and emission wavelengths. Therefore, a key requirement for efficient nonlinear frequency conversion in a plasmonic MS is to support phase-matched modes corresponding to the fundamental and nonlinearly generated optical waves. While phase matching (PM) (or momentum matching) between the fundamental input signal and the nonlinear output signal is considered a critical issue in photonic structures [30–32], it is often ignored in the design of nonlinear plasmonic structures. This is because the plasmonic structures strongly interact with a continuum of radiative waves, and therefore, a nonlinear signal can be generated by the interaction between a strong resonant mode for the fundamental input signal and matching radiative modes for the nonlinear signal. Previously, lattice plasmon (LP) structures [33–37] have been used to control and enhance high harmonic generation [38–43] and four-wave mixing [44] by supporting matching resonant modes for both the fundamental and nonlinear signals. However, most of the previous reports on nonlinear signal generation are based on only using a resonant fundamental wave and non-resonant radiative waves (for the nonlinearly generated wave). A comprehensive study of the effect of the relative phase between the fundamental and nonlinear modes in nanostructures that support sub-radiant plasmonic modes is lacking in the literature.

In this work, we show that the conversion efficiency in surface-enhanced second-harmonic generation (SESHG) in a strongly coupled nanoantenna array, supporting LP

***Corresponding authors: Hayk Harutyunyan,** Department of Physics, Emory University, Atlanta, GA 30322, USA, e-mail: hayk.harutyunyan@emory.edu; and
Ali Adibi, School of Electrical and Computer Engineering, Georgia Institute of Technology, Atlanta, GA 30332, USA, e-mail: ali.adibi@ece.gatech.edu
S. Hamed Shams Mousavi, Ali Eshaghian Dorche, Hossein Taheri and Ali A. Eftekhar: School of Electrical and Computer Engineering, Georgia Institute of Technology, Atlanta, GA 30332, USA
Robert Lemasters and Feng Wang: Department of Physics, Emory University, Atlanta, GA 30322, USA

modes for both fundamental and nonlinear signals, can be substantially improved in two ways by PM of the fundamental and second-harmonic LP modes. We will further show that using band-edge LP modes with zero momentum at the fundamental (also referred to as the pump) or second-harmonic frequency can lead to strong SESHG.

2 Results and discussion

The efficiency of second-harmonic generation in a medium depends on the wavevector mismatch between the fundamental (i.e. excitation) and second-harmonic (i.e. emission) waves, with frequencies f_1 and $f_2=2f_1$, and momenta $k_1(f_1)$ and $k_2(f_2)$, respectively, according to $I_2=I_{2,\max}\ \mathrm{sinc}^2\ (\Delta k\cdot L/2)$, with L being the interaction length and $\Delta k=2k_1-k_2$ [45]. In nonlinear crystals, often used in free-space nonlinear optics, the most common procedure is to use the material birefringence to achieve PM. Alternatively, in LP structures, the effective interaction length of the nonlinear process corresponds to the LP mode propagation length in the periodic plasmonic structure (e.g. ~50 μm). While the relatively short propagation length of LP modes relaxes the PM requirement, it still plays an important role in the efficiency of SESHG because of the strong dispersion of the LP modes. The PM condition in LP structures can be achieved by engineering the optical dispersion of the linear and second-harmonic waves (by engineering the LP structure geometry) to match at the desired fundamental frequency. This enables us to achieve high-conversion-efficiency SESHG in coupled plasmonic nanoantenna structures that support propagating LP modes, when the PM condition is satisfied.

To demonstrate the possibility of achieving PM between fundamental and second-harmonic LP modes, we develop a plasmonic nanoantenna array structure composed of a bilayer gold nanopillar-nanoaperture architecture, separated by dielectric pillars, as shown in Figure 1A. The structure is fabricated by patterning a thin (110-nm) layer of hydrogen silsesquioxane using electron-beam lithography to form a nanopillar array followed by deposition of a thin gold layer using electron-beam

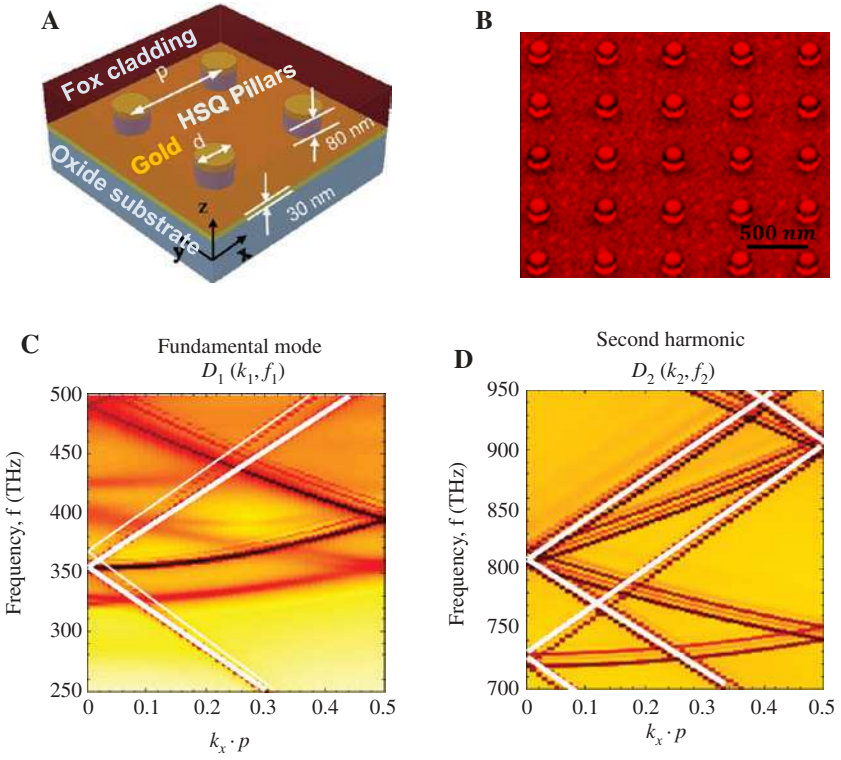

Figure 1: The LP nanostructure and its numerically calculated dispersion at the sweeping range of the excitation pump and the second-harmonic signal.
(A) Schematic view of the CPNA system based on coupled plasmonic (gold) nanoapertures and nanoantennas, separated with oxide dielectric pillars. (B) The SEM image of the nanostructure in (A) prior to coating with the cladding layer. The design parameters are $p=580$ nm and $d=160$ nm. (C) Band diagram of the structure in (A) at the envisioned fundamental frequency range (250–500 THz) for the structure periodicity, $p=520$ nm and (D) band diagram of the structure in (A) at the SHG frequency range (700–950 THz) for $p=580$ nm. The straight white lines are light lines of SiO_2 and FOX.

deposition and lift-off (see Supporting Information for the detailed fabrication process). This strongly coupled plasmonic nanoantenna supports LP modes, which can be tuned by adjusting the period of the array and the diameter of the nanopillars (p and d, respectively, in Figure 1A) [35]. Figure 1B shows a scanning electron microscopy (SEM) image of the fabricated nanostructure with a period of 580 nm and a nanopillar radius of 80 nm. The nanostructure is cladded with flowable oxide (FOX, PMCP17) to achieve stronger Fano resonances (with narrower line widths) associated with LP modes in the coupled plasmonic nanoparticle array (CPNA) structure [34, 36, 46]. Figure 1C and D shows the frequency dispersion of the fundamental and second-harmonic waves supported by this nanostructure, denoted by $D_1(f_1, k_1)$ and $D_2(f_2, k_2)$, respectively, calculated using the finite-difference time-domain method (Lumerical Inc.). As can be seen in Figure 1, this structure supports two LP modes in the range of 300–400 THz (Figure 1C), which is in the sweeping range of the pump laser (at the fundamental frequency) used in our measurements, and two additional LP modes in the range of 700–800 THz (Figure 1D), which is the range of the SHG signal. The white straight lines in these figures correspond to the light lines of SiO_2 and FOX.

To satisfy the PM condition, we should find matching points in the dispersion diagrams with $k_1 = k_2/2$ (we use k_1 and k_2 instead of k_{x1} and k_{x2}, respectively, for simplicity) and $f_1 = f_2/2$. To find these discrete sets of f's and k's, we have superimposed $D_1(2k_1, f_1)$ and $D_2(k_2, f_2/2)$ in Figure 2. The bands marked by blue lines in this figure show the dispersion relation of the fundamental mode stretched by a factor 2 in the direction of momentum, that is, $D_1(2k_1, f_1)$. All the other bands show the dispersion relation of the second-harmonic signal compressed by a factor 2 in the direction of frequency, that is, $D_2(k_2, f_2/2)$. From these superimposed dispersion diagrams, it is evident that the PM condition occurs at two discrete points, which are at the intersections of the higher fundamental LP band and the two second-harmonic LP bands, and they are approximately at: (a) $2\times k_1\, p = 0.58$ and $f_1 = 365$ THz ($\lambda_1 = 822$ nm), and (b) $2\times k_1\, p = 0.65$ and $f_1 = 370$ THz ($\lambda_1 = 810$ nm).

To experimentally investigate the effect of PM on the efficiency of SESHG, we have used an angle-resolved SHG measurement setup (see Supporting Information). Using this setup, the generated SHG corresponding to different points in the dispersion diagram can be measured by adjusting the pump frequency and the incident angle of the excitation wave (corresponding to the value of k_x). Briefly, a small diameter (~2 mm) laser beam from a Ti:sapphire oscillator source is first narrowed down to ~0.5 mm using a controllable slit and then focused on the sample using a high-numerical-aperture (NA = 1.42, oil immersion) objective lens. By adjusting the incident beam position with respect to the optical axis of the

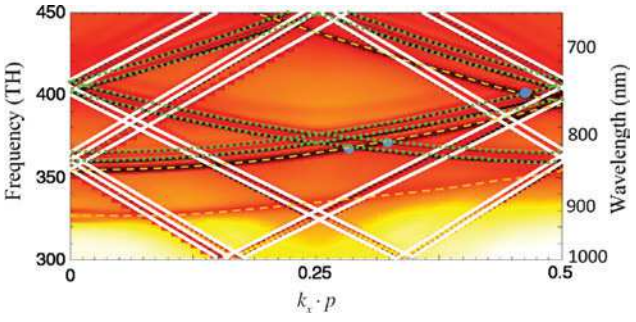

Figure 2: Phase matching between fundamental ($D_1(2k_1, f_1)$, slotted curves) and second-harmonic LP modes (dotted curves) for the structure in Figure 1B with $p = 580$ nm.
The second-harmonic bands are overlaid on the fundamental mode band structure by mapping the second-harmonic bands $D_2(k_2, f_2)$) on their equivalent excitation frequency and wavevector point on the dispersion diagram (i.e. $D_2(k_2/2, f_2/2)$). The phase-matching condition occurs at the intersection of the two dispersions (marked by blue dots), where $k_1 = k_2/2$ and $f_1 = f_2/2$, shown by blue dots: (1) Point A with $k_x p \sim = 0.27$, $f_1/\lambda_1 = 365$ THz/821 nm and Point B with $k_x p \sim = 0.32$, $f_1/\lambda_1 = 379$ THz/811 nm.

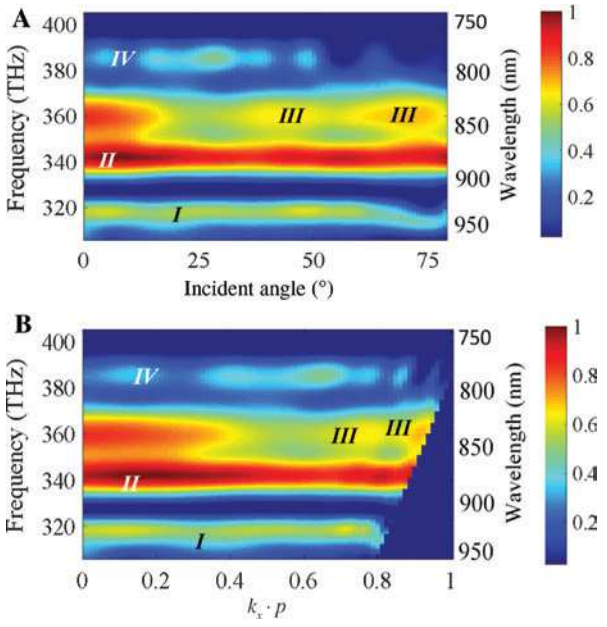

Figure 3: The measured normalized SESHG signal power (P_{SH}) versus the pump frequency (wavelength) and the excitation angle θ (A) and equivalent normalized in-plane wavevector (B), showing four important features: (I) a peak in SHG due to the first band edge of the fundamental LP mode, (II) a peak in SHG due to the second band edge of the fundamental LP mode, (III) two peaks in SHG due to PM and (IV) a peak in SHG due to the band edge of the second-harmonic LP mode.

objective (within the wide, ~11 mm, back aperture of the objective), the incident angle of light at the objective focal plane (and, therefore, the excitation wavevector) can be tuned over a wide range of angles (i.e. wavevectors). By moving the excitation beam position for ±4 mm from the objective center, an excitation angle dynamic range of $\theta \sim \pm 80°$ (corresponding to a normalized k_x of $\sim \pm 0.91$ in an LP structure with period $p = 580$ nm at the fundamental frequency of 350 THz) in the plasmonic structure cladding (FOX with a refractive index of 1.375) is achieved. The excitation beam size of ~0.5 mm also corresponds to an excitation beam width of ~5°. The same large-NA objective is used for the collection of the SHG signal and its subsequent detection with a CCD-coupled spectrometer. To calibrate the setup, we first measure the linear band structure of the CPNA using a wideband super-continuum source (Super-K) instead of the ultra-fast excitation source. The measured experimental results (shown in Figure S4, Supporting Information) show good agreement between the simulated and experimentally measured band structure of the fundamental mode. The results of the angle-resolved SHG measurements are presented in Figure 3 in the form of a heatmap, which shows the intensity of the SESHG signal measured with the pump wavelength varying from 740 nm (frequency ~405 THz) to 980 nm (frequency ~306 THz) and the excitation angle from $\theta = 0°$ to $\theta = 75°$. The surface second-order nonlinear susceptibility $\chi_s^{(2)}$ [19, 47, 48] between the gold (Au) layer and the top or bottom dielectrics is the primary source of SESHG in this nanostructure, as the bulk second-order nonlinearities of Au, SiO_2 and FOX at these wavelengths are quite negligible.

Four important features can be seen in the heatmap in Figure 3: (I) a peak at excitation wavelength (λ_p) ~940 nm (320 THz) in SESHG due to the first band edge of the fundamental LP mode, (II) a peak at ~880 nm (340 THz) due to the second band edge of the fundamental LP mode, (III) two peaks at $\lambda_p \sim 835$ nm (360 THz) and incident angles of 43° and 72° (corresponding to the set of f and k values that satisfy the PM condition) and (IV) a peak at the fundamental

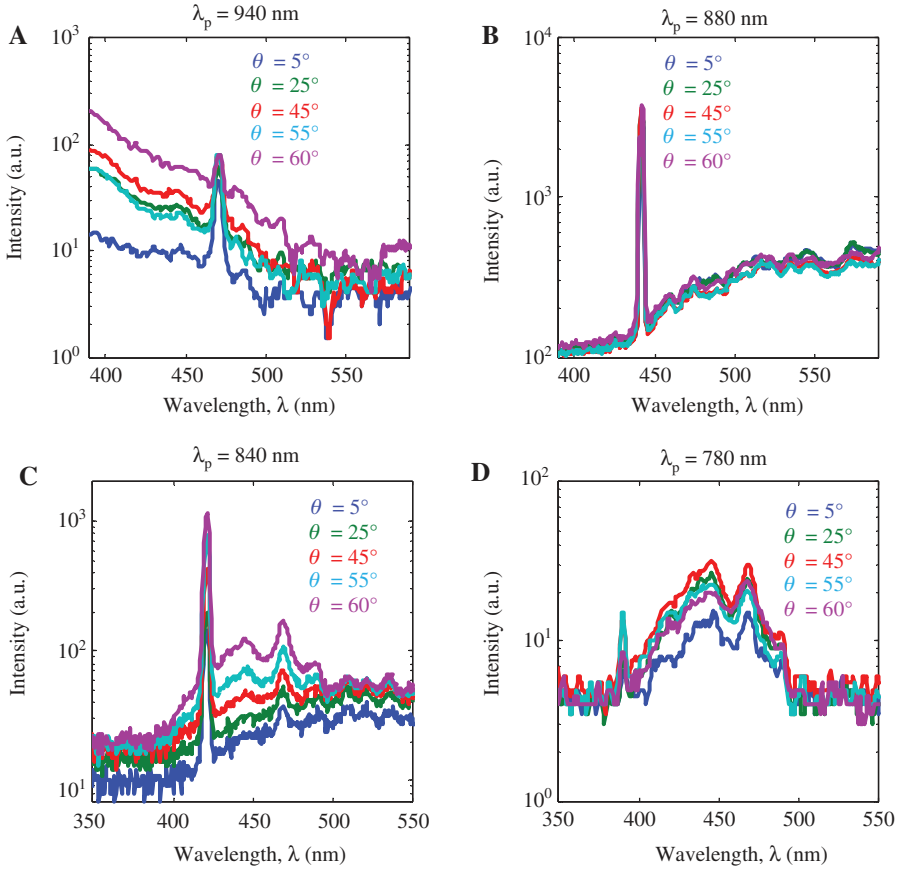

Figure 4: Evolution of the SESHG signal versus the excitation angle at the four critical excitation frequencies: (A) evolution of the SESHG peak at 470 nm near the first fundamental LP mode band edge, (B) evolution of the SESHG peak at 440 nm near the second fundamental LP mode band edge, (C) evolution of the SESHG peak at 420 nm near the PM wavelength and (D) evolution of the SESHG peak at 390 nm near the second-harmonic LP mode band edge. The (fundamental) pump wavelength in each case is shown by λ_p.

pump wavelength $\lambda_p \sim 780$ nm (385 THz) in SESHG due to the band edge of the second-harmonic LP mode.

The measured nonlinear spectra, including SESHG and the intrinsic two-photon excited photoluminescence (TPPL) of Au in the visible range [49, 50], at the frequencies of these four features are shown in Figure 4A–D for five different excitation angles (θ). These measured spectra have been corrected for the variable quantum efficiency of the photodetector and optical loss of the measurement system in the range of 380–500 nm (both shown in Supporting Information). The TPPL of Au is subtracted by fitting a polynomial curve to these spectra, and the intensity of the SESHG signal at the second-harmonic wavelength ($\lambda_p/2$) is reordered to generate the heatmap shown in Figure 3.

3 Conclusions

The results of Figures 3 and 4 show that an SESHG enhancement factor in the range of 10–100 can be achieved via PM (Figure 4C) or by using band-edge LP modes (Figure 4B). We believe that the same concept can be applied to the third-order and carrier-induced nonlinear optical effects to improve the conversation efficiency in third-harmonic generation, four-wave mixing and optical parametric oscillation, as well as improving the sensitivity in nonlinear spectroscopy and imaging.

Acknowledgments: This work was primarily funded by the Air Force Office of Scientific Research (AFOSR) under Grant No. FA9550-15-1-0342 (G. Pomrenke). This work was performed in part at the Georgia Tech Institute for Electronics and Nanotechnology (IEN), a member of the National Nanotechnology Coordinated Infrastructure, which is supported by the National Science Foundation under Grant No. ECCS-1542174. HH acknowledges support from NSF EFMA – 1741691 and Research Corporation for Science Advancement (24371).

References

[1] Foster MA, Turner AC, Sharping JE, Schmidt BS, Lipson M, Gaeta AL. Broad-band optical parametric gain on a silicon photonic chip. Nature 2006;441:960–3.
[2] Koos C, Vorreau P, Vallaitis T, et al. All-optical high-speed signal processing with silicon–organic hybrid slot waveguides. Nat Photonics 2009;3:216–9.
[3] Silberhorn C, Lam PK, Weiss O, König F, Korolkova N, Leuchs G. Generation of continuous variable Einstein-Podolsky-Rosen entanglement via the Kerr nonlinearity in an optical fiber. Phys Rev Lett 2001;86:4267–70.
[4] O'brien JL, Furusawa A, Vučković J. Photonic quantum technologies. Nat Photonics 2009;3:687–95.
[5] Sibson P, Erven C, Godfrey M, et al. Chip-based quantum key distribution. Nat Commun 2017;8:13984.
[6] Mousavi SS, Gallion P. Decoy-state quantum key distribution using homodyne detection. Phys Rev A 2009;80:012327.
[7] Scalora M, Dowling JP, Bowden CM, Bloemer MJ. Optical limiting and switching of ultrashort pulses in nonlinear photonic band gap materials. Phys Rev Lett 1994;73:1368–71.
[8] Steinmeyer G, Sutter D, Gallmann L, Matuschek N, Keller U. Frontiers in ultrashort pulse generation: pushing the limits in linear and nonlinear optics. Science 1999;286:1507–12.
[9] Zhang J, Lin Q, Piredda G, Boyd RW, Agrawal GP, Fauchet PM. Optical solitons in a silicon waveguide. Opt Express 2007;15:7682–8.
[10] Herr T, Brasch V, Jost JD, et al. Temporal solitons in optical microresonators. Nat Photonics 2014;8:145–52.
[11] Dudovich N, Oron D, Silberberg Y. Single-pulse coherently controlled nonlinear Raman spectroscopy and microscopy. Nature 2002;418:512–4.
[12] Camp Jr, CH, Lee YJ, Heddleston JM, et al. High-speed coherent Raman fingerprint imaging of biological tissues. Nat Photonics 2014;8:627–34.
[13] Zoumi A, Yeh A, Tromberg BJ. Imaging cells and extracellular matrix in vivo by using second-harmonic generation and two-photon excited fluorescence. Proc Natl Acad Sci USA 2002;99:11014–9.
[14] Campagnola PJ, Loew LM. Second-harmonic imaging microscopy for visualizing biomolecular arrays in cells, tissues and organisms. Nat Biotechnol 2003;21:1356–60.
[15] Freudiger CW, Min W, Saar BG, et al. Label-free biomedical imaging with high sensitivity by stimulated Raman scattering microscopy. Science 2008;322:1857–61.
[16] Kauranen M, Zayats AV. Nonlinear plasmonics. Nat Photonics 2012;6:737–48.
[17] Kachynski A, Pliss A, Kuzmin A, et al. Photodynamic therapy by in situ nonlinear photon conversion. Nat Photonics 2014;8:455–61.
[18] Huang X, Qian W, El-Sayed IH, El-Sayed MA. The potential use of the enhanced nonlinear properties of gold nanospheres in photothermal cancer therapy. Lasers Surg Med 2007;39:747–53.
[19] Shen Y. Surface properties probed by second-harmonic and sum-frequency generation. Nature 1989;337:519–25.
[20] Mesch M, Metzger B, Hentschel M, Giessen H. Nonlinear plasmonic sensing. Nano Lett 2016;16:3155–9.
[21] Yu R, Cox JD, de Abajo FJG. Nonlinear plasmonic sensing with nanographene. Phys Rev Lett 2016;117:123904.
[22] Zhang Y, Zhen Y-R, Neumann O, Day JK, Nordlander P, Halas NJ. Coherent anti-Stokes Raman scattering with single-molecule sensitivity using a plasmonic Fano resonance. Nat Commun 2014;5:4424.
[23] Yampolsky S, Fishman DA, Dey S, et al. Seeing a single molecule vibrate through time-resolved coherent anti-Stokes Raman scattering. Nat Photonics 2014;8:650–6.
[24] Harutyunyan H, Palomba S, Renger J, Quidant R, Novotny L. Nonlinear dark-field microscopy. Nano Lett 2010;10:5076–9.
[25] Palomba S, Novotny L. Near-field imaging with a localized nonlinear light source. Nano Lett 2009;9:3801–4.

[26] Kravtsov V, Ulbricht R, Atkin JM, Raschke MB. Plasmonic nano-focused four-wave mixing for femtosecond near-field imaging. Nat Nanotechnol 2016;11:459–64.
[27] Kim S, Jin J, Kim Y-J, Park I-Y, Kim Y, Kim S-W. High-harmonic generation by resonant plasmon field enhancement. Nature 2008;453:757–60.
[28] Park I-Y, Kim S, Choi J, et al. Plasmonic generation of ultrashort extreme-ultraviolet light pulses. Nat Photonics 2011;5:677–81.
[29] Sivis M, Duwe M, Abel B, Ropers C. Extreme-ultraviolet light generation in plasmonic nanostructures. Nat Phys 2013;9:304–9.
[30] Fiore A, Berger V, Rosencher E, Bravetti P, Nagle J. Phase matching using an isotropic nonlinear optical material. Nature 1998;391:463–6.
[31] Zhu S-N, Zhu Y-Y, Ming N-B. Quasi-phase-matched third-harmonic generation in a quasi-periodic optical superlattice. Science 1997;278:843–6.
[32] Berger V. Nonlinear photonic crystals. Phys Rev Lett 1998;81:4136.
[33] Zhou W, Odom TW. Tunable subradiant lattice plasmons by out-of-plane dipolar interactions. Nat Nanotechnol 2011;6:423–7.
[34] Vakevainen A, Moerland R, Rekola H, et al. Plasmonic surface lattice resonances at the strong coupling regime. Nano Lett 2013;14:1721–7.
[35] Shams Mousavi SH, Eftekhar AA, Atabaki AH, Adibi A. Band-edge bilayer plasmonic nanostructure for surface enhanced Raman spectroscopy. ACS Photonics 2015;2:1546–51.
[36] Auguié B, Barnes WL. Collective resonances in gold nanoparticle arrays. Phys Rev Lett 2008;101:143902.
[37] Rodriguez SRK, Abass A, Maes B, Janssen OT, Vecchi G, Rivas JG. Coupling bright and dark plasmonic lattice resonances. Phys Rev X 2011;1;021019.
[38] Walsh GF, Dal Negro L. Enhanced second harmonic generation by photonic–plasmonic Fano-type coupling in nanoplasmonic arrays. Nano Lett 2013;13:3111–7.
[39] Genevet P, Tetienne J-P, Gatzogiannis E, et al. Large enhancement of nonlinear optical phenomena by plasmonic nanocavity gratings. Nano Lett 2010;10:4880–3.
[40] Linden S, Niesler F, Förstner J, Grynko Y, Meier T, Wegener M. Collective effects in second-harmonic generation from split-ring-resonator arrays. Phys Rev Lett 2012;109:015502.
[41] Husu H, Siikanen R, Makitalo J, et al. Metamaterials with tailored nonlinear optical response. Nano Lett 2012;12:673–7.
[42] Thyagarajan K, Butet JRM, Martin OJ. Augmenting second harmonic generation using Fano resonances in plasmonic systems. Nano Lett 2013;13:1847–51.
[43] Li G, Chen S, Pholchai N, et al. Continuous control of the nonlinearity phase for harmonic generations. Nat Mater 2015;14:607–12.
[44] Renger J, Quidant R, Van Hulst N, Novotny L. Surface-enhanced nonlinear four-wave mixing. Phys Rev Lett 2010;104:046803.
[45] Boyd RW. Nonlinear optics. San Diego, CA, USA, Academic Press, 2003.
[46] Luk'yanchuk B, Zheludev NI, Maier SA, et al. The Fano resonance in plasmonic nanostructures and metamaterials. Nat Mater 2010;9:707–15.
[47] Chen C, de Castro ARB, Shen Y. Surface-enhanced second-harmonic generation. Phys Rev Lett 1981;46:145.
[48] Simon H, Mitchell D, Watson J. Optical second-harmonic generation with surface plasmons in silver films. Phys Rev Lett 1974;33:1531.
[49] Bouhelier A, Bachelot R, Lerondel G, Kostcheev S, Royer P, Wiederrecht G. Surface plasmon characteristics of tunable photoluminescence in single gold nanorods. Phys Rev Lett 2005;95:267405.
[50] Wang H, Huff TB, Zweifel DA, et al. In vitro and in vivo two-photon luminescence imaging of single gold nanorods. Proc Natl Acad Sci USA 2005;102:15752–6.

Supplementary Material: The online version of this article offers supplementary material (https://doi.org/10.1515/nanoph-2018-0181).